Unintentional bulk doping of polymer-fullerene blends from a thin interfacial layer of MoO3

Nyman, Mathias; Dahlström, Staffan; Sandberg, Oskar; Österbacka, Ronald

Published in:
Advanced Energy Materials

DOI:
10.1002/aenm.201600670

Published: 01/01/2016

Document Version
(Peer reviewed version when applicable)

DOI: 10.1002/aenm.201600670
Article type: Full Paper

Unintentional Bulk Doping of Polymer-Fullerene Blends from a Thin Interfacial Layer of MoO_3

Mathias Nyman, Staffan Dahlström, Oskar J. Sandberg, and Ronald Österbacka**

Dr. M. Nyman, S. Dahlström, O. J. Sandberg, Prof. R. Österbacka

Physics/Faculty of Science and Engineering, and Center for Functional Materials, Åbo Akademi University, Porthansgatan 3, 20500 Turku, Finland
E-mail: mathnyma@abo.fi, rosterba@abo.fi

Keywords: organic solar cells, charge selective layers, unintentional doping

Charge selective interlayers are of critical importance in order for solar cells based on low mobility materials, such as polymer-fullerene blends, to perform well. Commonly used anode interlayers consist of high work function transition metal oxides, with molybdenum trioxide (MoO_3) being arguably the most used. Here we show that a thin interlayer of MoO_3 causes unintentional bulk doping in solar cells based on polymers and polymer-fullerene blends. The doping concentrations determined from capacitance-voltage measurements are larger than 10^{16} cm^{-3} and are seen to increase closer to the anode, reference devices without MoO_3 are undoped. Using time of flight secondary ion mass spectroscopy (ToF-SIMS) we furthermore show that molybdenum is present on the surface of all films with an interfacial layer of MoO_3 beneath the active layer. Doping concentrations of this magnitude are detrimental for device performance, especially for active layers > 100 nm.

1. Introduction

Recent progress in the field of organic photovoltaics has resulted in improved charge transport properties and reduced bulk recombination with a concomitant increase in efficiency. As losses to bulk recombination decreases, surface recombination, i.e. extraction of the wrong

type of charge carrier, will be an increasingly important loss mechanism[1]. In order to ensure efficient extraction of majority carriers and reduce surface recombination, charge selective interlayers are typically introduced[2, 3]. For anodes this is typically done by inserting a thin layer of a high work function metal oxide, such as MoO_3, which makes the anode ohmic for holes and prevents extraction of electrons with increased efficiency as a result[4-8]. MoO_3 is usually applied using thermal evaporation, but solution processed MoO_3 films have also been reported[9, 10].

Despite recent progress the mobility is still comparatively low in organic solar cell materials, and a built-in electric field is needed in order to extract carriers efficiently. A potentially detrimental effect on device performance stems from unintentional doping of the active layer due to impurities. Impurities may be a result of the manufacturing process, but they may also come from migration of molecules from the contacts[11-15]. Doping results in the formation of a depletion region (at the cathode, in case of uniform p-doping) with width w_0 at zero applied voltage given by:

$$w_0 = \sqrt{\frac{2\varepsilon\varepsilon_0\left(V_{bi}-\frac{kT}{q}\right)}{qN_p}} \quad (1)$$

where ε is the relative dielectric constant, ε_0 is the vacuum permittivity, V_{bi} is the built-in potential, k is the Boltzmann constant, T is the temperature, q is the elementary charge and N_p is the doping concentration. If the doping concentration is high enough, such that w_0 is smaller than the device thickness d, the entire potential drop in the device will occur over the depletion region, leaving the rest of the semiconductor layer charge-neutral and field-free. This leads to efficient extraction of (photo)generated charges only in the depletion region, whereas charges generated in the neutral region will have a large probability of recombining due to the lack of sufficient driving force for extraction[16-20]. A higher doping concentration leads to a thinner depletion region which in turn leads to lower photocurrent generation. In

addition, impurities in the active layer may result in charge carrier trapping with a concomitant decrease in the mobility and increase in trap-assisted recombination.

The doping concentrations are typically determined from impedance spectroscopy using Mott-Schottky analysis[21-23]. We recently demonstrated that the charge extraction by a linearly increasing voltage (CELIV) technique can be used to determine the doping concentrations and built-in potentials in sandwich type devices, given that the doping concentration is high enough so that the depletion region width w_0 is smaller than the device thickness d [24]. A schematic of the technique is shown in **Figure 1**. A linearly increasing voltage pulse $V(t) = A \cdot t$ is applied in reverse direction with slope $A = V_{max}/t_{pulse}$, where V_{max} is the maximum voltage and t_{pulse} is the time of the pulse. Provided that A is low enough, such that t_{pulse} is much larger than the charge carrier transit time, the resulting current transient $j(t)$ will be directly determined by the depletion layer capacitance $C_w = \frac{\varepsilon\varepsilon_0}{w}$ and given by: $j(t) = C_w \frac{dV}{dt}$. Assuming p-doping with uniform concentration N_p the current transient reads[24]:

$$j(t) = \frac{\sqrt{\frac{qN_p\varepsilon\varepsilon_0}{2}}}{\sqrt{At+V_{bi}-\frac{kT}{q}}}A \qquad (2)$$

It should be noted that the only difference to (low frequency) impedance spectroscopy is that CELIV is a time-domain measurement whereas impedance spectroscopy is in the frequency-domain.

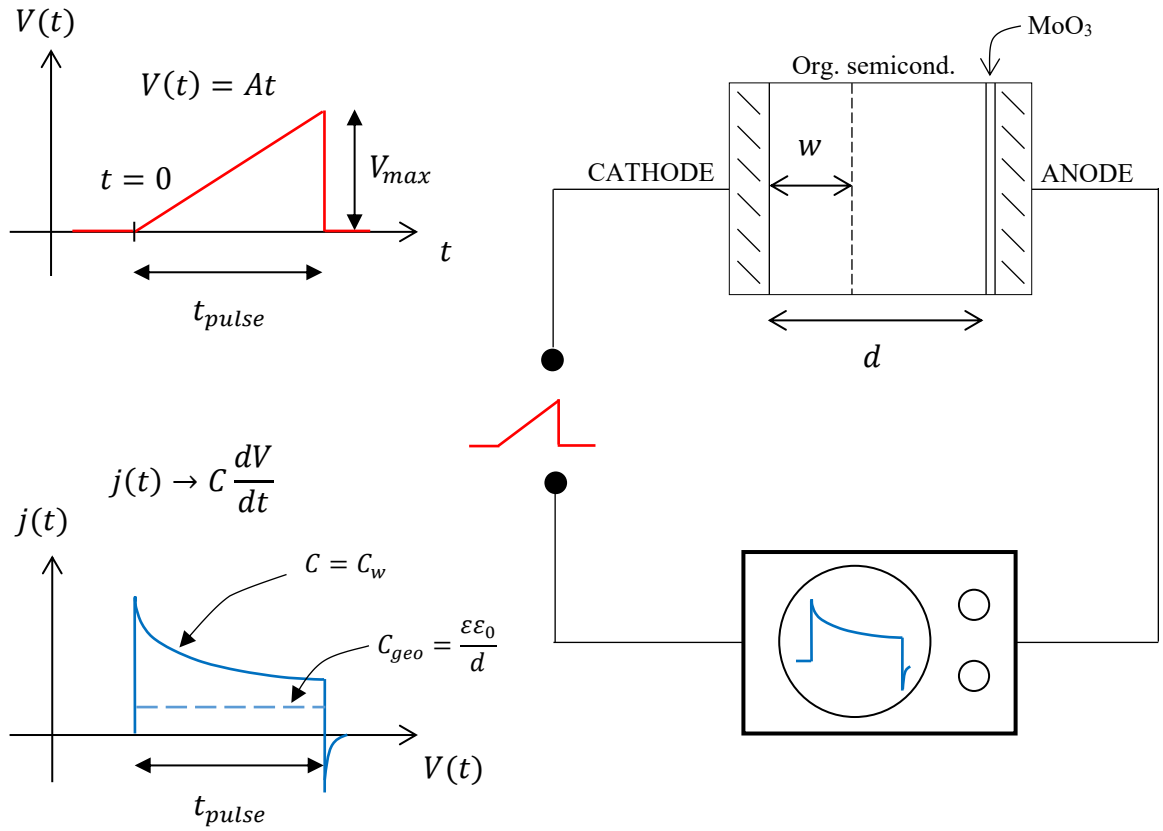

Figure 1 Organic semiconductors used in sandwich-typed diode structures are inherently undoped. If a high enough concentration of p-dopants is introduced into the semiconductor layer, a Schottky junction of thickness $w < d$ is formed at the cathode-semiconductor contact. In this case the steady-state capacitance of the device is given by the depletion layer capacitance C_w. By applying a linearly increasing voltage pulse with $A = V_{max}/t_{pulse}$ in reverse bias, the capacitance can be determined from the resulting extraction current transients approaching $j(t) = C\frac{dV}{dt}$ at large t_{pulse}. In case of an undoped device, the capacitance is closely given by the geometrical capacitance C_{geo}.

As model systems we use the conjugated polymers Poly(3-hexylthiophene) (P3HT) and poly[2,5-bis(3-tetradecylthiophen-2-yl)thieno[3,2-b]thiophene] (PBTTT). The ionization potentials are 4.45 eV[25] and 5.1 eV[26], respectively. Both pure polymer and bulk-heterojunction blends with [6,6]-phenyl-C61-butyric acid methyl ester (PCBM) or indene-C_{60} bis-adduct (ICBA) are studied.

2. Results and Discussion

Figure 2 a) shows the current transients of an ITO/MoO_3/P3HT:PCBM/LiF/Al device and a reference device without MoO_3, the transients are normalized to the displacement current $j_0 = AC_{geo}$ from the charging of the geometrical capacitance $C_{geo} = \frac{\varepsilon\varepsilon_0}{d}$. The device without MoO_3 has an almost flat response with $j \approx j_0$ indicating no or very low doping concentration. The current transient is very similar to those previously reported on similar devices but with MoO_3 replaced by PEDOT:PSS[17, 27]. A fully depleted device should have $j \equiv j_0$, however, in general there are always a small amount of charge present in the active layer due to diffusion from the contacts or Fermi-level pinning, especially in thin films with ohmic contacts[27, 28] but typically j does not exceed $1.5 \cdot j_0$. In contrast, the device with the MoO_3 interlayer shows a drastically increased current response due to an increased doping concentration with $j > 7 \cdot j_0$. The observed current transient is in excellent agreement with equation (2) with $N_p = 6 \cdot 10^{16}$ cm^{-3} (shown as a dashed line).

In the doping induced capacitive regime i.e. when $j = A \cdot C_w$, the doping profile $N_p(w)$ can be determined as[21]:

$$N_p(w) = \frac{2}{q\epsilon\epsilon_0 A^2}\left[\frac{d}{dV}(1/j(V)^2)\right]^{-1} \quad (3)$$

where $V = A \cdot t$ is the transient applied voltage and $w = \frac{\epsilon\epsilon_0 A}{j(t)}$. In theory, by applying an offset voltage equal to the built-in potential, and a voltage slope such that at V_{max} the device is fully depleted ($w = d$), the doping profile of the whole active layer can be obtained. However, in practice this will not be possible due to charge injection at large applied voltages. The corresponding doping profile for the ITO/MoO_3/P3HT:PCBM/LiF/Al device is shown in **Figure 2 c)**. The doping profile is surprisingly uniform with a slight increase in doping concentration for increasing w (closer to the anode). Also the dark IV curves (Supplementary information) show a drastic increase in the currents with the addition of the MoO_3 layer. This

can partly be due to the increased charge carrier density in the active layer, however, the main effect most probably is that ITO/MoO_3 makes an ohmic contact to P3HT whereas ITO does not.

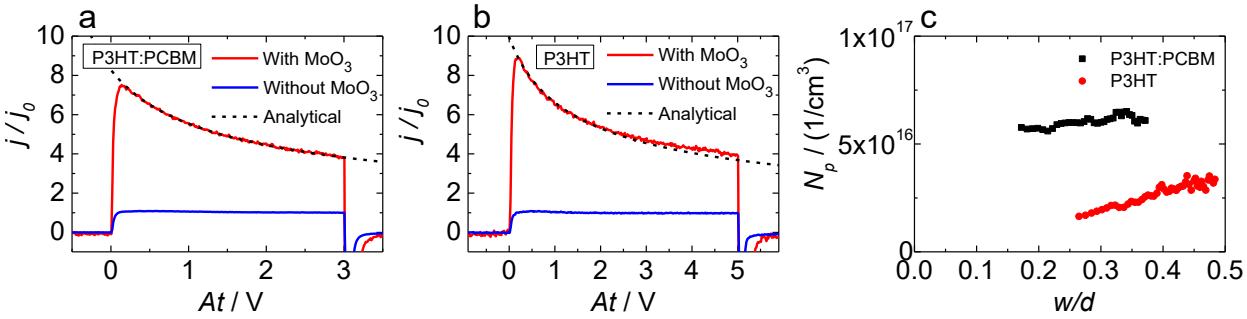

Figure 2 Normalized current transients of (a) an ITO/MoO_3/P3HT:PCBM/LiF/Al device and a reference device without MoO_3 (active layer thickness 470 nm) and (b) an ITO/MoO_3/P3HT/Al device and a reference device without MoO_3 (active layer thickness 800 nm). In (c) the corresponding doping profiles as a function of *w*/*d* (with respect to the cathode) for the devices with MoO_3 are shown.

It has been suggested that a high work function anode may cause doping of the active layer due to Fermi-level alignment[29, 30]. J. Wang et al observed doping of the P3HT:PCBM active layer stretching 200 nm into the bulk[29]. They suggested that the cause of the doping is charge transfer from the contact into the active layer in accordance with the Integer Charge Transfer (ICT) model[30]. Spontaneous charge transfer into discrete interfacial states have been shown at both metal-organic and organic-organic interfaces[30, 25], however, it is unclear how charges originating from charge transfer at the contact-active layer interface would cause doping this far into the active layer, and give rise to a nearly uniform doping profile.

Two independent groups have shown that the band bending in pure P3HT stretches only ~ 10 nm from the contact into the active layer[30, 32]. **Figure 2 b)** shows the current transients of a thick P3HT-device with and without MoO_3. Similar to the P3HT:PCBM case the doping concentration is below the detection limit when no MoO_3 is used, whereas the doping concentration is drastically increased with the addition of an interfacial layer of MoO_3. The

fitting to Equation 2 is not as good as in the P3HT:PCBM case, the reason is the non-uniform doping profile as seen in Figure 2 c). The doping concentration increases linearly for increasing depletion region thickness (towards the anode), however, the doping concentration is > 10^{16} cm^{-3} 600 nm from the anode and it is highly unlikely that this could be caused by spontaneous charge transfer at the anode-active layer interface.

We propose that the origin of the fixed space charge is MoO_3 molecules diffusing into the active layer, acting as dopants. In order to test this hypothesis we performed ToF-SIMS measurements on P3HT:PCBM films, with and without an interfacial layer of MoO_3 on the bottom. The results show a clear difference between the MoO_3 device and the reference, as seen in **Figure 3**. The red shaded areas show the positions of the seven most abundant Mo isotope masses, while the height of the bars is adjusted to the relative occurrence of each isotope (in arbitrary units). The difference in the ToF-SIMS spectra shows that Mo is present on the surface of the ITO/MoO_3/P3HT:PCBM film indicating that MoO_3 has migrated through the whole active layer. ToF-SIMS is a qualitative measurement and quantitative information is difficult or impossible to obtain the absolute level of Mo present on the surface.

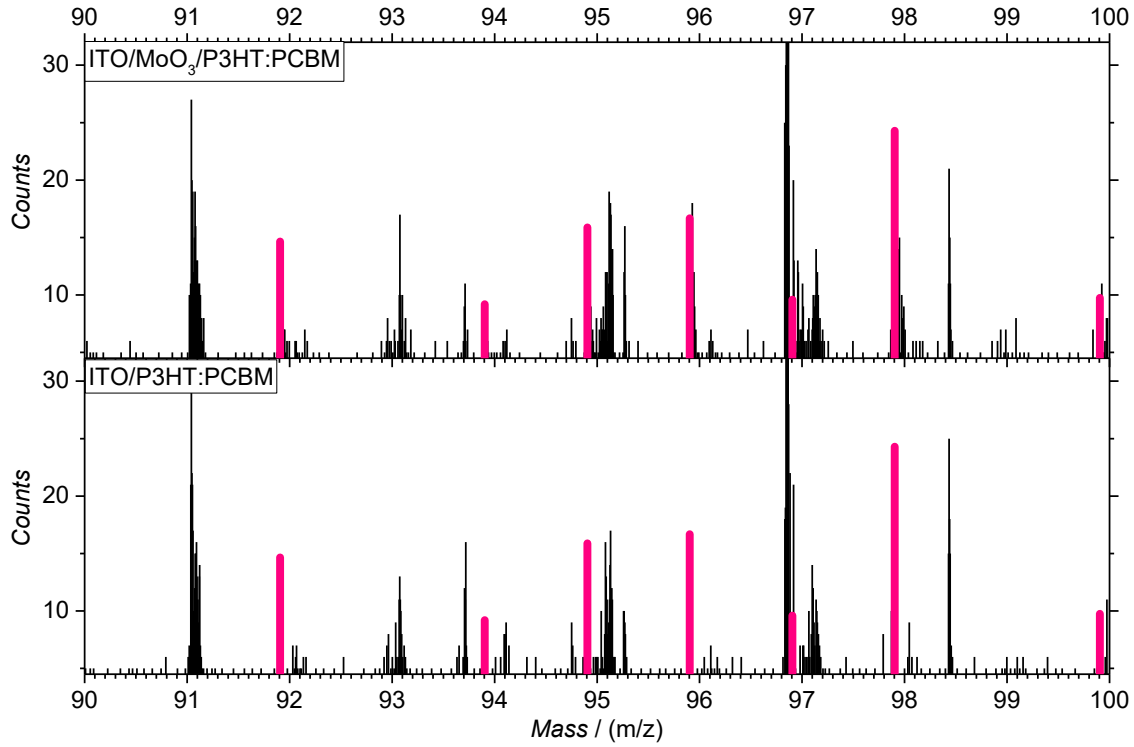

Figure 3 ToF-SIMS data from the surface of an ITO/MoO_3/P3HT:PCBM and an ITO/P3HT:PCBM film (film thickness 180 nm). The red shaded areas show the relative occurrence of the seven most common Mo isotopes.

The fact that MoO_3 molecules cause doping in P3HT is obvious given the high electron affinity of MoO_3[8]. What is surprising is that MoO_3 molecules diffuse from an evaporated 2 nm thick layer at the anode through the whole active layer causing an almost uniform doping in P3HT:PCBM. A. Dai et al have previously demonstrated the diffusion of solution processed p-dopants based on Mo-complexes in polymer and polymer-fullerene films[33]. However, in their case the dopant is soluble and introduced in the polymer solution before spin-coating. They furthermore noted that the dopants are much more mobile in pure P3HT than in P3HT:ICBA. In our case the diffusion appears to be easier in P3HT:PCBM than in pure P3HT, given the uniform and high doping concentration in P3HT:PCBM. The diffusibility of MoO_3 clearly depends on the properties of the active layer, such as the morphology.

In order to show the generality of this phenomenon, and to demonstrate the effect of different morphologies, we performed similar measurements on the polymer PBTTT. PBTTT was chosen due to its high structural order and low trap density when blended with PCBM[34,35]. The ToF-SIMS spectra for PBTTT and PBTTT:PCBM with and without MoO_3 are shown in the Supporting Information, Mo is seen on the surface of both films with MoO_3. The doping profile for PBTTT:PCBM is similar to that of P3HT; the doping concentration is seen to increase linearly towards the anode in the device with MoO_3, as shown in **Figure 4**, whereas the device without MoO_3 shows no doping. Compared to the P3HT:PCBM case the doping concentration is somewhat lower and markedly less uniform. Figure 4 also shows the doping profile for a P3HT:ICBA device, which is seen to be fairly similar to the P3HT:PCBM case.

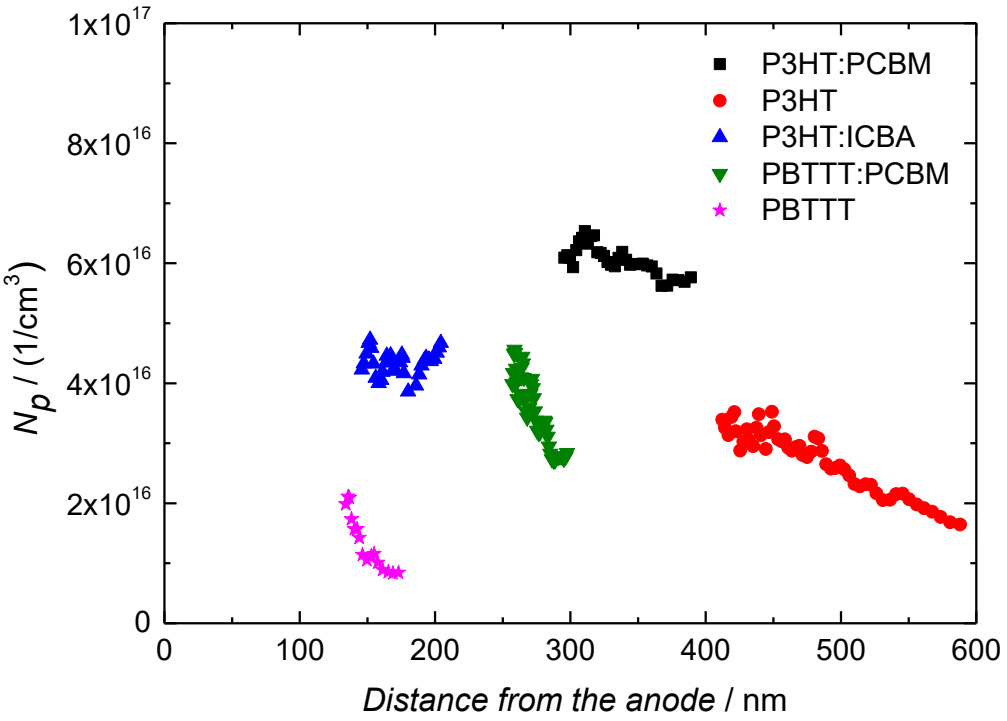

Figure 4 Measured doping profiles in devices with different polymer-fullerene blends and a MoO_3-modified anode. The device thicknesses are 470 nm (P3HT:PCBM), 800 nm (P3HT), 420 nm (P3HT:ICBA), 490 nm (PBTTT:PCBM) and 492 nm (PBTTT). Reference devices without MoO_3 are undoped.

In the systems studied here MoO_3 is least mobile in pure PBTTT, the doping concentration is below $2 \cdot 10^{16}$ cm^{-3}. Furthermore it can be seen from the doping profile that the dopants are located fairly close to the anode and decreasing sharply towards the cathode. It seems that the addition of PCBM facilitates the diffusion of MoO_3 into the active layer most likely due to the spherical symmetry and smaller size of the fullerene compared to the polymers. However, we note that the current transients in the PBTTT case are not perfectly capacitive which makes determination of the doping concentration less reliable (Supporting Information).

We have thus far shown that molecules from a thin layer of MoO_3 on the bottom anode in conventional structures migrate into the active layer causing doping. Furthermore, we have good reason to believe MoO_3 diffuses into the active layer also when evaporated on top of the active layer, in an inverted structure[36]. In order to demonstrate this we fabricated a device with sub-monolayer (2 Å) of MoO_3 between the active layer and the Al top contact. Also in this case, an increased doping concentration is seen compared with reference devices without MoO_3 (Supporting Information). However, due to the low MoO_3 concentration (due to the very thin MoO_3 layer) the concentration and doping profile is challenging to determine. Devices with thicker MoO_3 at the cathode were not possible to measure due to the very large leakage currents.

We believe that this effect is general to all bulk-heterojunction blends, although the concentration of diffused MoO_3 will depend on several factors including active layer composition, morphology, processing, and ageing of the devices. In addition, the doping efficiency might be different in materials with different energetics. The doping concentrations reported here results in depletion regions around 100 nm, in thin devices the depletion region might be thicker than the active layer and in this case the device will be effectively undoped. However, the MoO_3 will still accept electrons, given the high electron affinity, resulting in weakened charge transport properties and an increased trap-assisted recombination. When w_0

< *d*, part of the active layer will be field-free which affects the performance negatively, since charges generated in the neutral region will not contribute significantly to the current[19, 20]. This is especially detrimental for devices in the standard architecture, i.e. bottom (transparent) anode and top (reflective) cathode since the depletion region will be formed at the cathode whereas the intensity of the incoming light is highest at the anode, which leads to a highly thickness dependent efficiency in these types of devices[19]. In order to make bulk-heterojunction solar cells viable for large scale production using printing techniques a thickness independent efficiency is highly desirable for reliable manufacturing on low-cost substrates.

It is not unlikely that also other metal oxides, such as V_2O_5 and WO_3, will penetrate into the active layer, given their similar structures. This implies that modifying contacts in organic photovoltaic devices with high electron affinity metal oxides is a fundamentally problematic device design, and highlights the importance of developing alternative charge selective layers.

3. Conclusion

Unintentional bulk doping in diodes and solar cells based on polymers and polymer-fullerene blends is clarified using capacitance-voltage measurements. The unintentional doping is shown to be caused by MoO_3 diffusing from a thin interfacial layer through the whole active layer, which is verified by ToF-SIMS measurements. The doping concentrations are determined to be larger than 10^{16} cm^{-3}, which is highly detrimental for device performance.

Experimental Section

Samples were prepared as follows; ITO covered borosilicate glass (from Präzisions Glas & Optik GmbH) was used as substrate. Half of the substrate was etched with HCl for roughly 40 minutes. The substrates were subsequently cleaned in a 1:1:5 blend of H_2O_2, NH_3 and water in an ultrasonicator at 80° C for 30 minutes. A layer of 2 nm MoO_3 (Sigma-Aldrich) was evaporated on the ITO prior to spin-casting of the active material. Films containing P3HT

were spin-cast from 50 mg/ml solution in chlorobenzene and annealed at 120 ˚C for 15 minutes. PBTTT and PBTTT:PCBM films were spin-cast from di-chlorobenzene solutions with a concentration of 40 mg/ml and 60 mg/ml respectively. Subsequently a 0.8 nm layer of LiF followed by 60 nm of Al was thermally evaporated as a top contact. Samples for ToF-SIMS were made using the same procedure leaving out the evaporated top contact. The active material was spin-cast from solutions of lower concentration to achieve thinner films in these samples. Reference samples were made similarly without the MoO_3 layer. Spin-coating, annealing and thermal evaporation was carried out in a nitrogen glovebox. The active layer thicknesses were determined using atomic force microscopy.

CELIV measurements were performed as reported earlier[24, 36]. In the case of p-doping a depletion region is formed at the cathode with thickness (at zero applied voltage) w_0 given by equation (1). When applying a linearly increasing voltage pulse with slope A in reverse direction on a p-doped Schottky-diode such that $w_0 < d$, the extraction current transient $j(t)$ will be purely capacitive (for slow pulses) and given by:[24]

$$j(t) = C_w \frac{dV}{dt} \tag{4}$$

The depletion region as a function of time is then given by:

$$w = \frac{\epsilon\epsilon_0 A}{j(t)} \tag{5}$$

By plotting j^{-2} the built in potential and doping concentration can be determined, furthermore, the doping profile $N_p(w)$ can be determined by Equation 3 (see Supporting Information). In the undoped case the current transient will simply be given by the displacement current from the charging of the geometrical capacitance $j_0 = \frac{A\varepsilon\varepsilon_0}{d}$.

Time of Flight Secondary Ion Mass Spectrometry (ToF-SIMS) measurements were performed at Top Analytica Ltd. with Physical Electronics TRIFT II using 15 kV Ga-ions. The measurements were optimized for detecting positive Mo-ions. The analyzed area was 200 µm × 200 µm and the acquisition time was 10 min.

Supporting Information
Supporting Information is available from the Wiley Online Library or from the author.

Acknowledgements
The Academy of Finland is acknowledged for funding through project #279055.

[1] O. J. Sandberg, A. Sundqvist, M. Nyman, R. Österbacka, *Phys. Rev. Applied* **2016**, *5*, 044005.

[2] R. Po, C. Carbonera, A. Bernardi, and N. Camaioni, *Energy Environ. Sci.* **2011**, *4*, 285.

[3] H. Zeng, X. Zhu, Y. Liang, X. Guo, Polymers **2015**, *7*, 333.

[4] V. Shrotriya, G. Li, Y. Yao, C.-W. Chu, Y. Yang, *Appl. Phys. Lett.* **2006**, *88*, 073508.

[5] A. K. K. Kyaw, X. W. Sun, C. Y. Jiang, G. Q. Lo, D. W. Zhao, D. L. Kwong, *Appl. Phys. Lett*. **2008**, *93*, 221107.

[6] Y. Sun, C. J. Takacs, S. R. Cowan, J. H. Seo, X. Gong, A. Roy, A. J. Heeger, *Adv. Mater.* **2011**, *23*, 2226.

[7] Y.-H. Lou, Z.-K. Wang, D-X. Yuan, H. Okada, L.-S. Liao, *Appl. Phys. Lett.* **2014**, *105*, 113301.

[8] J. Meyer, S. Hamwi, M. Kröger, W. Kowalsky, T. Riedl, A. Kahn, *Adv. Mater.* **2012**, *24*, 5408.

[9] C. Girotto, E. Voroshazi, D. Cheuns, P. Heremans, B. P. Rand, *ACS Appl. Mater. Interfaces* **2011**, 3, 3244.

[10] G. Wang, T. Jiu, P. Li, Jun Li, C. Sun, F. Lu, J. Fang, *Solar Energy Materials & Solar Cells* **2014**, *120*, 603.

[11] G. Zhang, *PhD Thesis*, University of California, Los Angeles, USA, **2015**.

[12] K. Suemori, M. Yokoyama, M. Hiramoto, *J. Appl. Phys.* **2006**, *99*, 036109.

[13] S. Chambon, L. Derue, M. Lahaye, B. Pavageau, L. Hirsch, G. Wantz, *Materials* **2012**, *5*, 2521.

[14] W. R. Mateker, J. D. Douglas, C. Cabanetos, I. T. Sachs-Quintana, J. A. Bartelt, E. T. Hoke, A. El Labban, P. M. Beaujuge, J. M. J. Fréchet, M. D. McGehee, *Energy Environ. Sci.* **2013**, *6*, 2529.

[15] G. Zhang, S. A. Hawks, C. Ngo, L. T. Schelhas, D. T. Scholes, H. Kang, J. C. Aguirre, S. H. Tolbert, B. J. Schwartz, *ACS Appl. Mater. Interfaces* **2015**, *7*, 25247.

[16] F. Deledalle T. Kirchartz, M. S. Vezie, M. Campoy-Quiles, P. S. Tuladhar, J. Nelson, J. R. Durrant, *Phys. Rev. X* **2015**, *5*, 011032.

[17] A. Seemann, T. Sauermann, C. Lungenschmied, O. Armbruster, S. Bauer, H.-J. Egelhaaf, and J. Hauch, *Sol. Energy* **2011**, *85*, 1238.

[18] A.J. Morfa, A.M. Nardes, S.E. Shaheen, N. Kopidakis, J. van de Lagemaat, *Adv. Funct. Mater.* **2011**, *21*, 2580.

[19] T. Kirchartz, T. Agostinelli, M. Campoy-Quiles, W. Gong, J. Nelson, *J. Phys. Chem. Lett.* **2012**, *3*, 3470.

[20] G. F. A. Dibb, M.-A. Muth, T. Kirchartz, S. Engmann, H. Hoppe, G. Gobsch, M. Thelakkat, N. Blouin, S. Tierney, M. Carrasco-Orozco, J. R. Durrant, J. Nelson, *Sci. Rep.* **2013**, *3*, 3335.

[21] S.M. Sze, *Physics of Semiconductor Devices*, Wiley& Sons, New York, USA, **1981**.

[22] E.J. Lous, P.W.M. Blom, L.W. Molenkamp, D.M. Leeuw, *Phys. Rev. B* **1995**, *51*, 17251.

[23] T. Kirchartz, W. Gong, Steven A. Hawks, T. Agostinelli, R. C. I. MacKenzie, Y. Yang, J. Nelson, *J. Phys. Chem. C* **2012**, *116*, 7672.

[24] O. J. Sandberg, M. Nyman, R. Österbacka, *Org. Electron.* **2014**, *15*, 3413.

[25] H. Aarnio, P. Sehati, S. Braun, M. Nyman, M. P. de Jong, M. Fahlman, R. Österbacka, *Adv. Energy Mater.* **2011**, *1*, 792.

[26] I. McCulloch et al, "Liquid-crystalline semiconducting polymers with high charge-carrier mobility", *Nat. Mater.* **2006**, *5*, 328.

[27] M. Nyman, F. Pettersson, R. Österbacka, *Chem. Phys.* **2012**, *404*, 60.

[28] S. L. M. Mensfoort, R. Coehoorn, *Phys. Rev. Lett.* **2008**, *100*, 086802.

[29] J. Wang, L. Xu, Y.-J. Lee, M. De Anda Villa, A. V. Malko, J. W. P. Hsu, *Nano Lett.* **2015**, *15*, 7627.

[30] R. C. Shallcross, T. Stubhan, E. L. Ratcliff, A. Kahn, C. J. Brabec, N. R. Armstrong, *J. Phys. Chem. Lett.* **2015**, *6*, 1303.

[31] S. Braun, W. R. Salaneck, M. Fahlman, *Adv. Mater.* **2009**, *21*, 1450.

[32] Q. Bao, S. Fabiano, M. Andersson, S. Braun, Z. Sun, X. Crispin, M. Berggren, X. Liu, M. Fahlman, *Adv. Funct. Mater*. **2016**, *26*, 1077.

[33] A. Dai, A. Wan, C. Magee, Y. Zhang, S. Barlow, S. R. Marder, A. Kahn, *Org. Electron.* **2015**, *23*, 151.

[34] M. Nyman, O. J. Sandberg, R. Österbacka, *Synth. Met.* **2015**, *201*, 6.

[35] M. Nyman, O. J. Sandberg, R. Österbacka, *Adv. Energy Mater.* **2015**, *5*, 1400890.

[36] A. Sundqvist, O. J. Sandberg, M. Nyman, J.-H. Smått, R. Österbacka, *Adv. Energy Mater.* **2016**, *6*, 1502265.

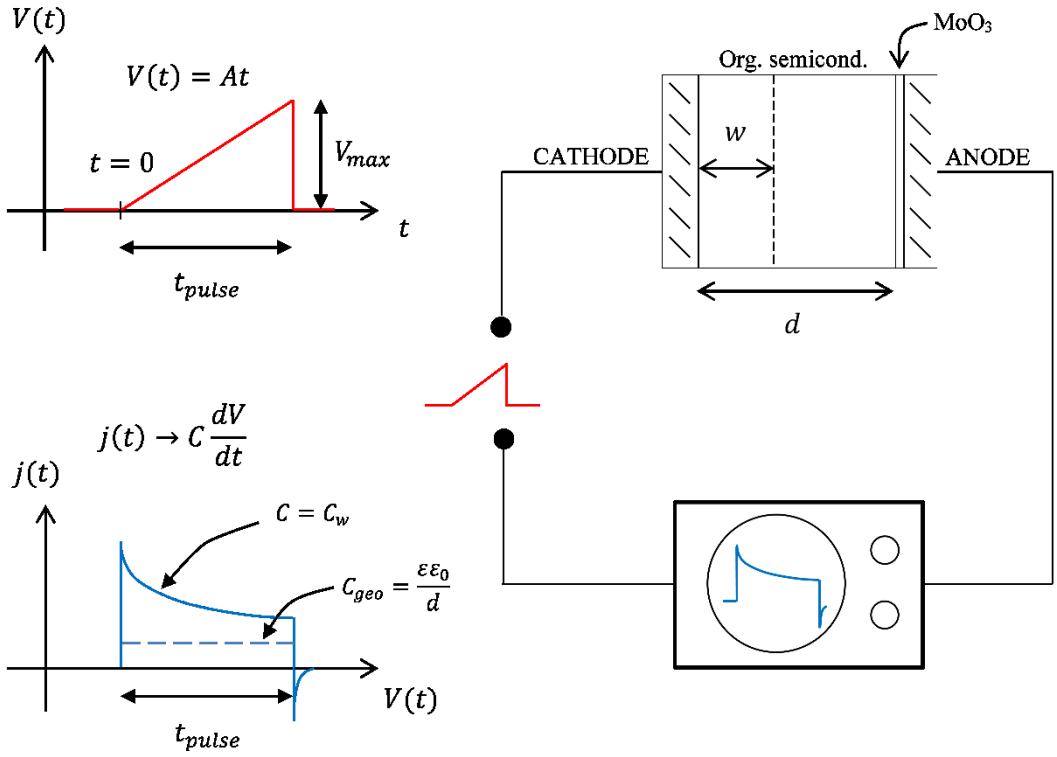

Figure 1 Organic semiconductors used in sandwich-typed diode structures are inherently undoped. If a high enough concentration of p-dopants is introduced into the semiconductor layer, a Schottky junction of thickness $w < d$ is formed at the cathode-semiconductor contact. In this case the steady-state capacitance of the device is given by the depletion layer capacitance C_w. By applying a linearly increasing voltage pulse with $A = V_{max}/t_{pulse}$ in reverse bias, the capacitance can be determined from the resulting extraction current transients approaching $j(t) = C\frac{dV}{dt}$ at large t_{pulse}. In case of an undoped device, the capacitance is closely given by the geometrical capacitance C_{geo}.

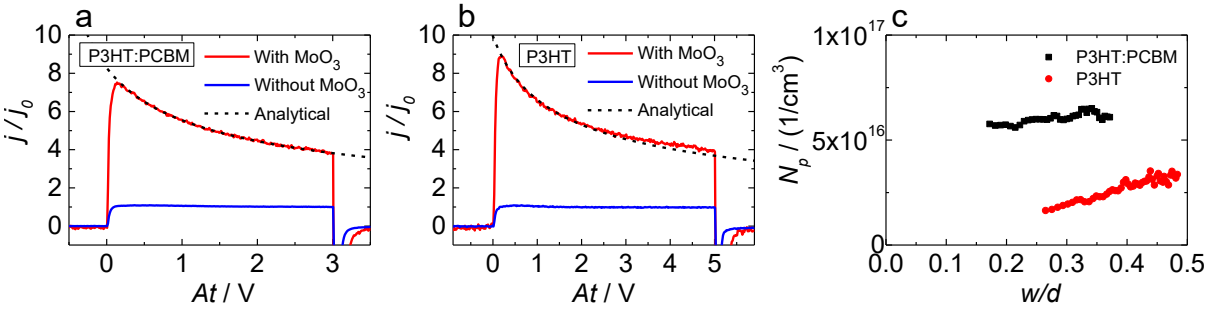

Figure 2 Normalized current transients of (a) an ITO/MoO_3/P3HT:PCBM/LiF/Al device and a reference device without MoO_3 (active layer thickness 470 nm) and (b) an ITO/MoO_3/P3HT/Al device and a reference device without MoO_3 (active layer thickness 800 nm). In (c) the corresponding doping profiles as a function of *w*/*d* (with respect to the cathode) for the devices with MoO_3 are shown.

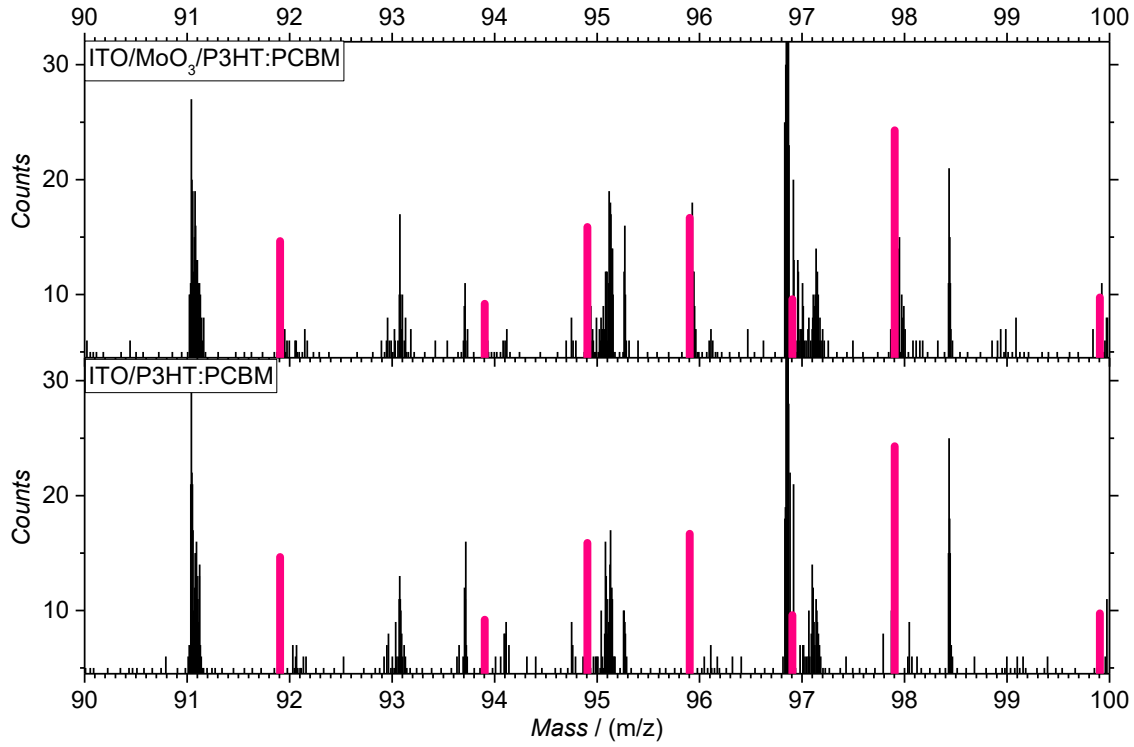

Figure 3 ToF-SIMS data from the surface of an ITO/MoO_3/P3HT:PCBM and an ITO/P3HT:PCBM film (film thickness 180 nm). The red shaded areas show the relative occurrence of the seven most common Mo isotopes.

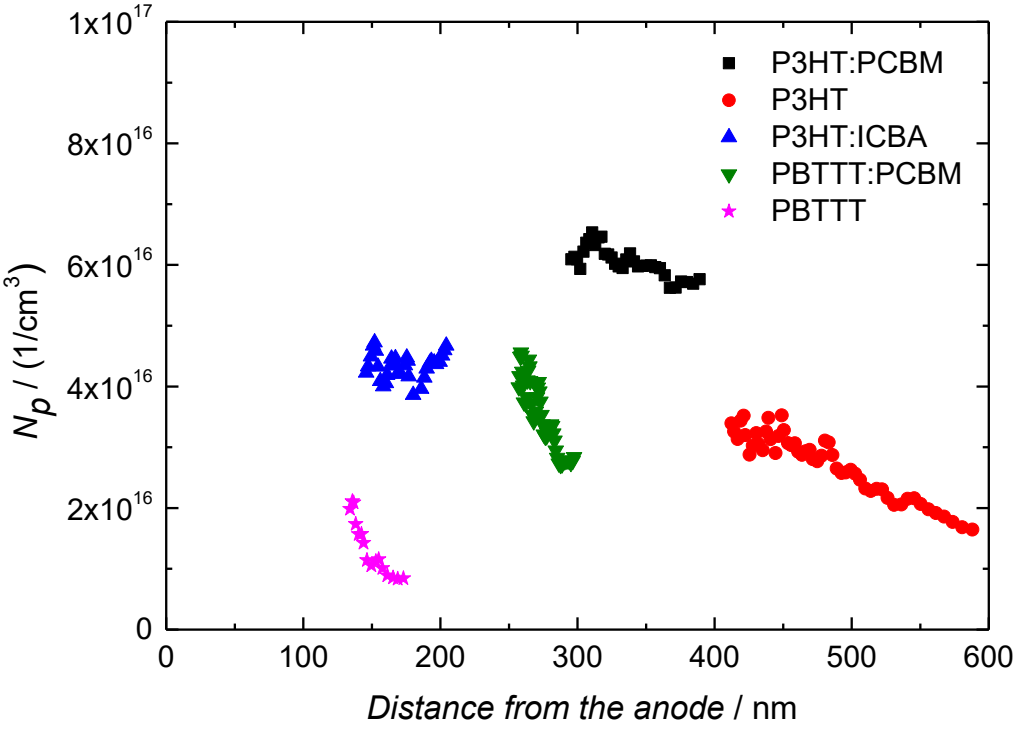

Figure 4 Measured doping profiles in devices with different polymer-fullerene blends and a MoO_3-modified anode. The device thicknesses are 470 nm (P3HT:PCBM), 800 nm (P3HT), 420 nm (P3HT:ICBA), 490 nm (PBTTT:PCBM) and 492 nm (PBTTT). Reference devices without MoO_3 are undoped.

Supporting Information

Unintentional bulk doping of polymer-fullerene blends from a thin interfacial layer of MoO_3

Mathias Nyman, Staffan Dahlström, Oskar J. Sandberg, and Ronald Österbacka**

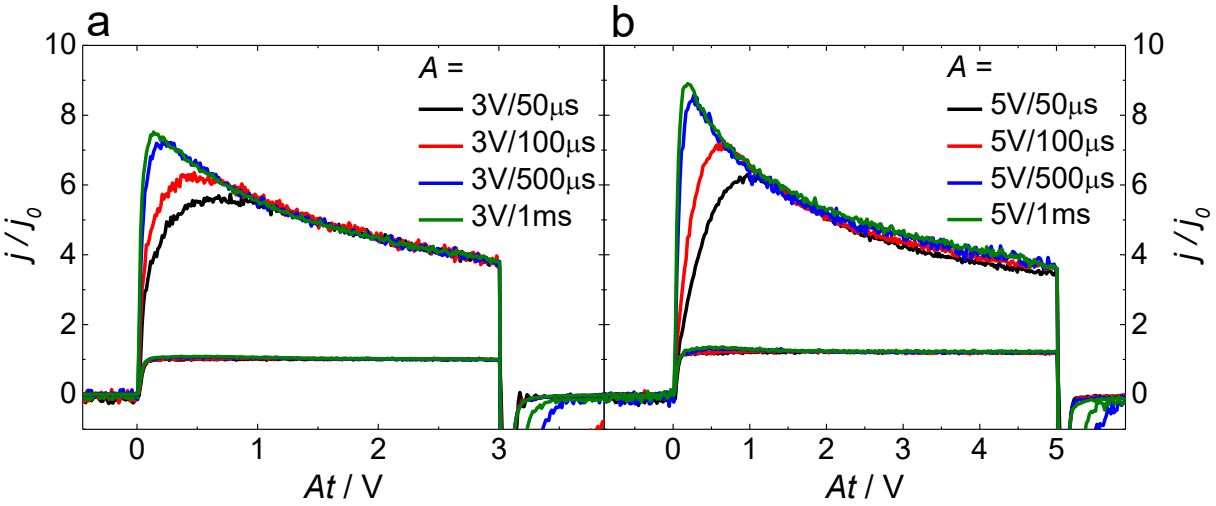

Figure S1 CELIV transients with varying voltage slope A normalized to j_0 of (a) an ITO/P3HT:PCBM/LiF/Al and an ITO/MoO_3/P3HT:PCBM/LiF/Al device (active layer thickness 470 nm) and (b) an ITO/P3HT/Al and an ITO/MoO_3/P3HT/Al device (active layer thickness 800 nm).

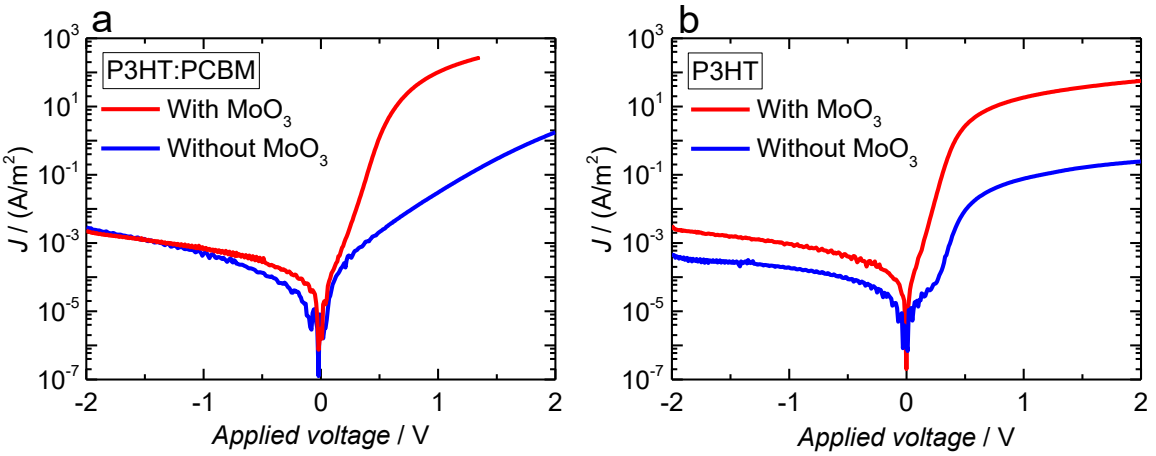

Figure S2 Dark IV curves of (a) an ITO/P3HT:PCBM/LiF/Al and an ITO/MoO_3/P3HT:PCBM/LiF/Al device and (b) an ITO/P3HT/Al and an ITO/MoO_3/P3HT/Al device.

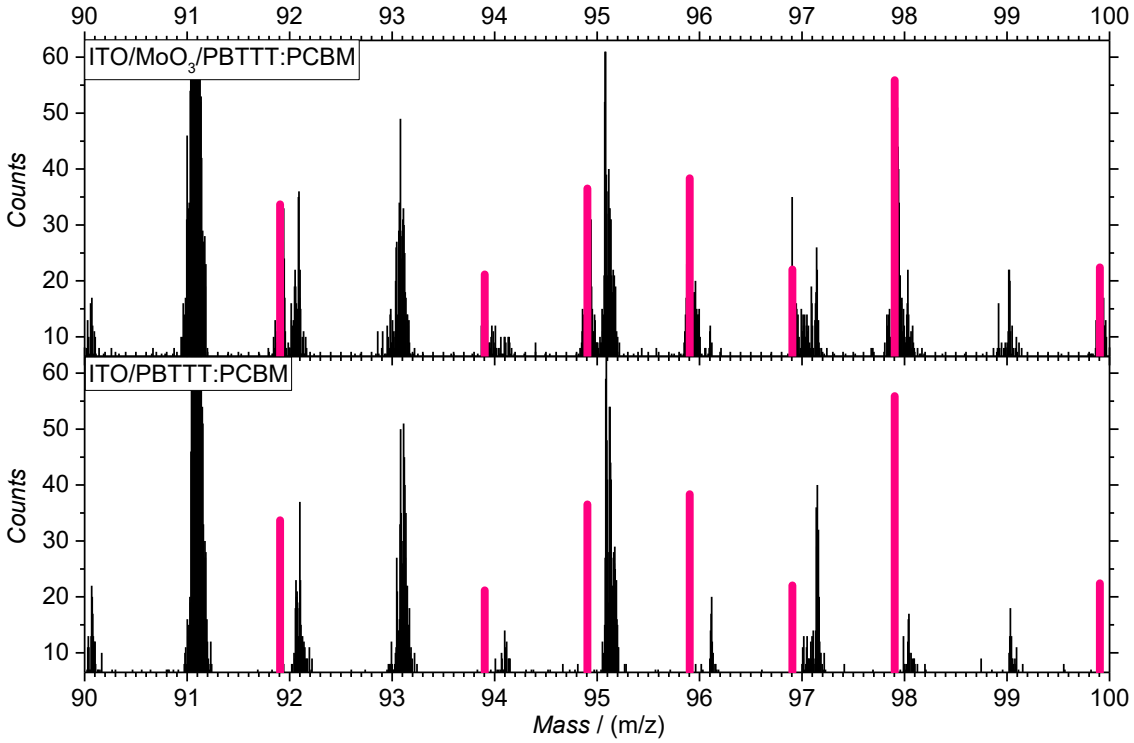

Figure S3 ToF-SIMS data from the surface of an ITO/PBTTT:PCBM and an ITO/MoO_3/PBTTT:PCBM film (film thickness 105 nm).

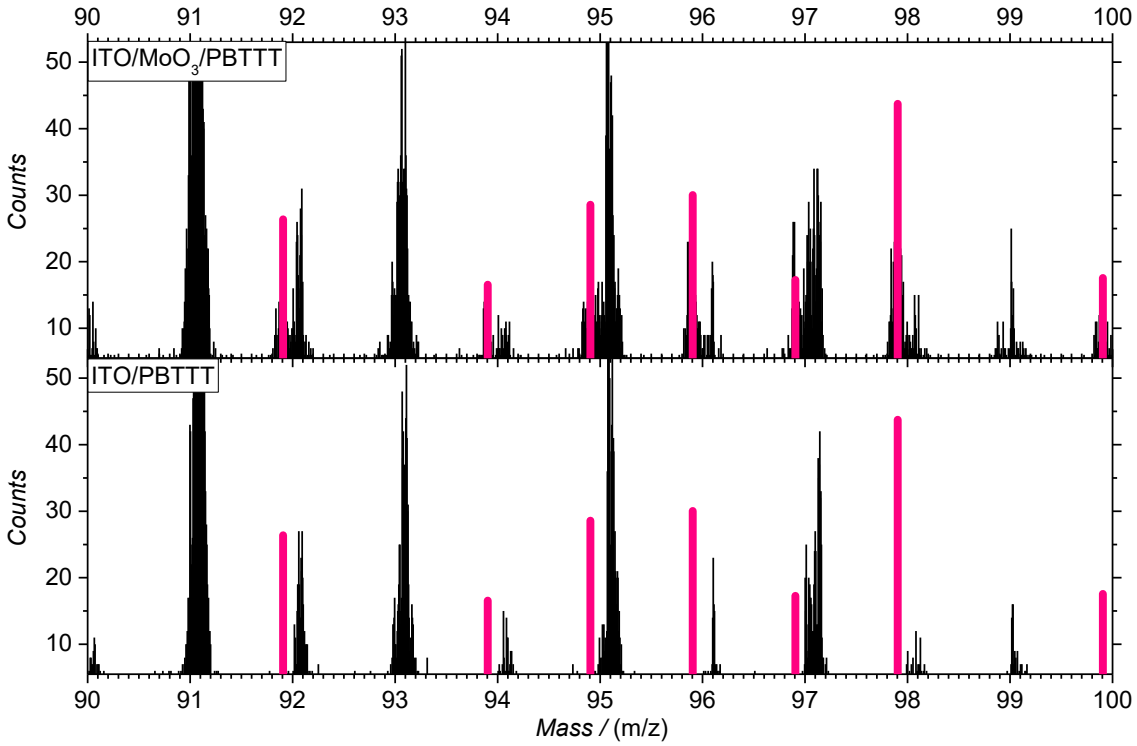

Figure S4 ToF-SIMS data from the surface of an ITO/PBTTT and an ITO/MoO_3 /PBTTT film (film thickness 191 nm).

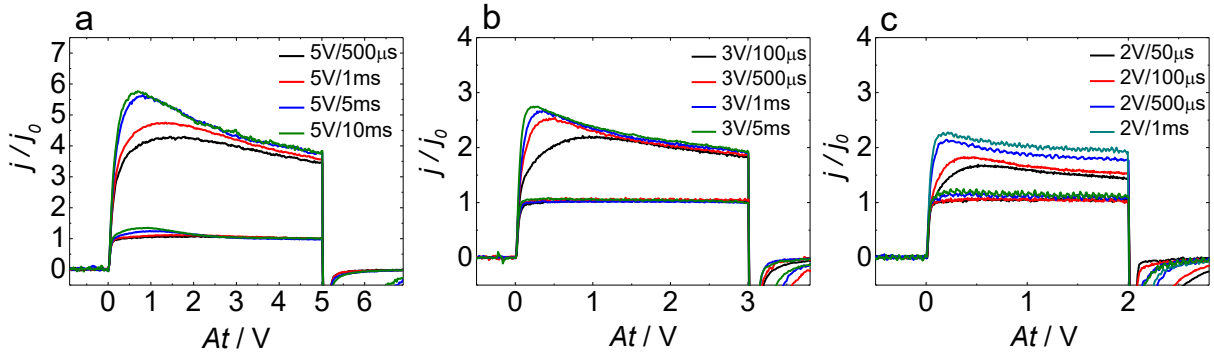

Figure S5 CELIV transients with varying voltage slope A normalized to j_0 of (a) an ITO/P3HT:ICBA/LiF/Al and an ITO/MoO_3/P3HT:ICBA/LiF/Al device (active layer thickness 420 nm) , (b) an ITO/PBTTT:PCBM/LiF/Al and an ITO/MoO_3/PBTTT:PCBM/LiF/Al device (active layer thickness 490 nm) and (c) an ITO/PBTTT/LiF/Al and an ITO/MoO_3/PBTTT/LiF/Al device (active layer thickness 492 nm).

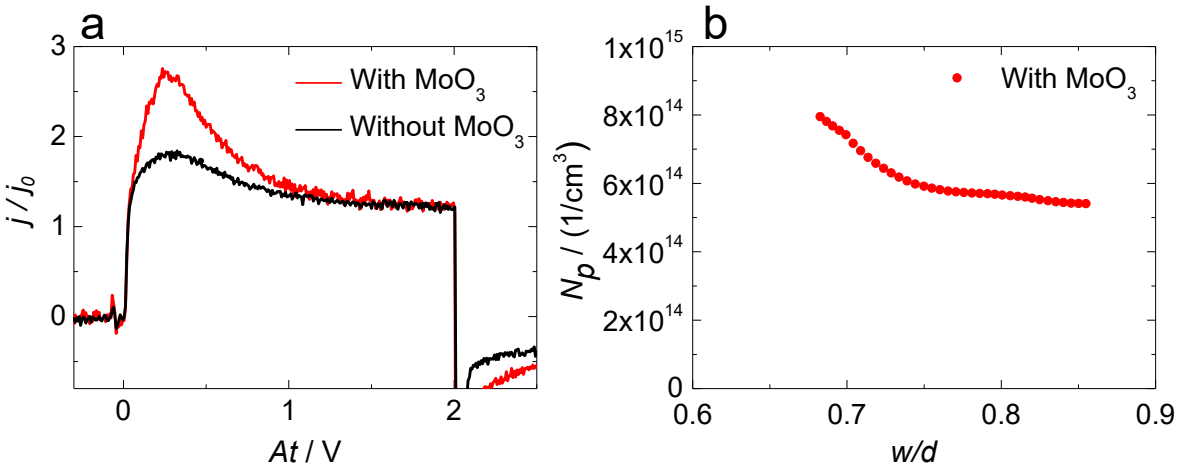

Figure S6 (a) CELIV transients normalized to j_0 of an Au/P3HT /Al and an Au/P3HT/MoO_3/Al device (active layer thickness 845 nm) (b) The corresponding doping profile.